Gelation threshold of cross-linked polymer brushes

Max Hoffmann,[1,2] Michael Lang,[1] and Jens-Uwe Sommer[1,2]
[1]*Leibniz Institute of Polymer Research Dresden e.V., Hohe Straße 6, D-01069 Dresden, Germany*
[2]*Technische Universtät Dresden, Institute for Theoretical Physics, D-01069 Dresden, Germany*
(Received 15 November 2010; published 23 February 2011)

The cross-linking of polymer brushes is studied using the bond-fluctuation model. By mapping the cross-linking process into a two-dimensional (2D) percolation problem within the lattice of grafting points, we investigate the gelation transition in detail. We show that the particular properties of cross-linked polymer brushes can be reduced to the distribution of bonds which are formed between the grafted chains, and we propose scaling arguments to relate the gelation threshold to the chain length and the grafting density. The gelation threshold is lower than the percolation threshold for 2D bond percolation because of the longer range and broad distribution of bonds formed by the cross-linking process. We term this type of percolation problem *star percolation*. We observe a broad crossover from mean-field to critical percolation behavior by analyzing the cluster size distribution near the gelation threshold.

DOI: 10.1103/PhysRevE.83.021803 PACS number(s): 82.35.Gh, 68.47.Mn, 64.60.ah

I. INTRODUCTION

Polymer brushes consist of polymer chains grafted to a surface with one end. The chains stretch out due to the excluded-volume interactions, when grafted densely enough, resembling the bristles of a brush. The stretching leads to a behavior of the chains in a brush different from free chains, which led to a variety of applications ranging from colloid stabilization [1,2] to drug delivery [3]. Polymer brushes are also used for the reduction of friction [4–6], increasing the biocompatibility of medical implants [7], and as switchable amphiphilic surfaces [8,9].

A first theoretical model for polymer brushes based on mean-field and scaling concepts was given by Alexander and de Gennes [10–12]. Here, each chain forms a string of excluded volume blobs whose extension is given by the grafting density. Using self-consistent field approaches, a refined description of the monomer profile inside the brush has been obtained by Semenov [13] and Milner *et al.* [14]. Computer simulations have also been applied by several groups to test theoretical models and to explore detailed static and dynamic properties of polymer brushes [15–21]. On the experimental side, great progress has been made over the years [22] with recent accomplishments allowing very high grafting densities to be examined [23].

In many applications, polymer brushes are situated on surfaces that are exposed to a sometimes harsh environment. This exposure and the resulting interactions with the polymer brush lead to a slow destruction of the brush, because more and more chains are broken or torn away from the substrate. Introducing cross-links inside the brush provides a solution to this destruction problem: Should a chain degraft, then it can be connected to other chains so that it remains inside the brush. Such a cross-linking approach has been taken, for instance, in [24,25]. Another application of cross-linking of grafted chains is to freeze a certain state of the brushes under given solvent conditions, which has recently been applied for switchable brushes [8]. On the other hand, cross-linking a polymer brush leads to a novel type of polymer network, since the chains to be cross-linked are stretched and ordered. Furthermore, a cross-linked polymer brush represents an ultrathin quasi-two-dimensional polymer network, where the thickness is given by the extension of a single chain only. To the best of our knowledge there is no computational or theoretical study of cross-linked polymer brushes up to now.

In this work we use the bond-fluctuation model (BFM) to simulate polymer brushes and the cross-linking process. The model has been proven to be successful for simulating cross-linked polymers [26–29]. In order to investigate the gelation properties in detail, we map the cross-linking process into a percolation problem on the 2D lattice of grafting points. This mapping allows the realization of large systems that could otherwise not be investigated. The key property of the original problem to be transferred to the percolation problem is the distribution of bond vectors obtained in the cross-linking process. This procedure leads to a particular type of percolation problem that we call *star percolation* - as motivated by the structure of the connections in the grid of grafting points. We study the properties of the bond vector distribution and reveal a scaling variable, which controls this distribution for different chain lengths and grafting densities. Using the star percolation model, we investigate the percolation threshold and the distribution of cluster sizes at the critical point of percolation.

The remainder of the work is organized as follows: The simulation model and the cross-linking process are described in Sec. II. The mapping of the cross-linking process onto the 2D percolation problem is explained in Sec. II B. Network properties are discussed in Sec. III A, while the bond distribution and its scaling properties are analyzed in Sec. III B. Star percolation and its basic properties are introduced in Sec. IV and its application to the gelation problem of polymer brushes is presented in Sec. V. We give a summery and our conclusions in Sec. VI.

II. SIMULATION MODEL AND PERCOLATION ANALYSIS

A. Bond-fluctuation model and cross-linking process

The bond-fluctuation model was first introduced by Carmesin and Kremer in 1988 [30] in order to simulate conformations and dynamics of dense polymer systems with

excluded volume interactions. The simulations in this work were performed with the version of the BFM algorithm proposed by Deutsch and Binder [31]. The BFM does not consider hydrodynamic interactions and the solvent is treated implicitly in the athermal limit. In this model, the monomers are represented by cubes on a regular cubic lattice with each cube occupying eight lattice positions, which cannot be shared with another cube (excluded volume). The monomers of one chain are connected by a bond vector out of a predefined vector set. The combination of bond vector set and excluded volume of monomers in this model ensures cut avoidance of strands without an explicit test of the local topology [31].

In the early 1990s Sommer et al. [26,32] showed that the BFM is well suited to capture static and dynamic properties of polymer networks. For the purpose of this publication, the BFM as described in [31] is augmented with a cross-linking process for the polymer brushes. During the course of the simulation, cross-linking between two (not directly connected) monomers can be initiated by a face-to-face collision between the two monomers. Instead of rejecting the move, the following conditions are checked: The new bond does not exceed the maximum functionality of $f = 3$ for each monomer and an activation barrier for cross-linking is checked by a Metropolis-type algorithm as described in [32]. Here, a probability (rate of cross-linking) is chosen for a successful formation of the cross-link. As a result, a network builds up in time and the network information is stored in a *bond list*. Once established bonds are assumed to be stable and thus are kept permanently.

We simulated the cross-linking of polymer brushes with chain lengths $N = 16$, 32, and 64 and grafting densities $\sigma = 0.04$, 0.0625, 0.11, 0.1588, and 0.25. The unit of the grafting density is the inverse squared BFM lattice constant, where $\sigma = 1$ corresponds to the maximum possible grafting density in the BFM model. System sizes varied between approximately 1500 and 10 000 grafting points and periodic boundary conditions were applied in the xy direction. Reflecting boundary conditions were used in the z direction and the grafting plane corresponds to $z = 0$. The grafting points are arranged regularly on a square lattice. The brush was created in a fully stretched configuration and was then relaxed for much longer than the relaxation time τ_R to obtain totally independent and relaxed start configurations for the cross-linking and measurement runs. The overlap threshold for the grafting density, σ^*, has been estimated from the scaling analysis of the brush height for the various chain lengths after being completely relaxed. Here, we have identified the overlap density as the crossing point of the asymptotic brushlike and mushroomlike behaviors of the height of the brush as a function of σ. The cross-linking rate was set to unity (immediate cross-linking). Supplementary simulations have shown that the results do not alter even if the cross-linking rate is lowered by a factor of 10 or even more.

B. The percolation problem

The result of the cross-linking process is a bond list, which contains the cross-links established during the network formation. Before we analyze the bond list further we need to define the percolation problem for cross-linked polymer brushes. To be in line with the original bond percolation problem all bonds which cross the simulation box boundaries (due to the periodic boundary conditions used in the simulation) were eliminated from the bond list first.

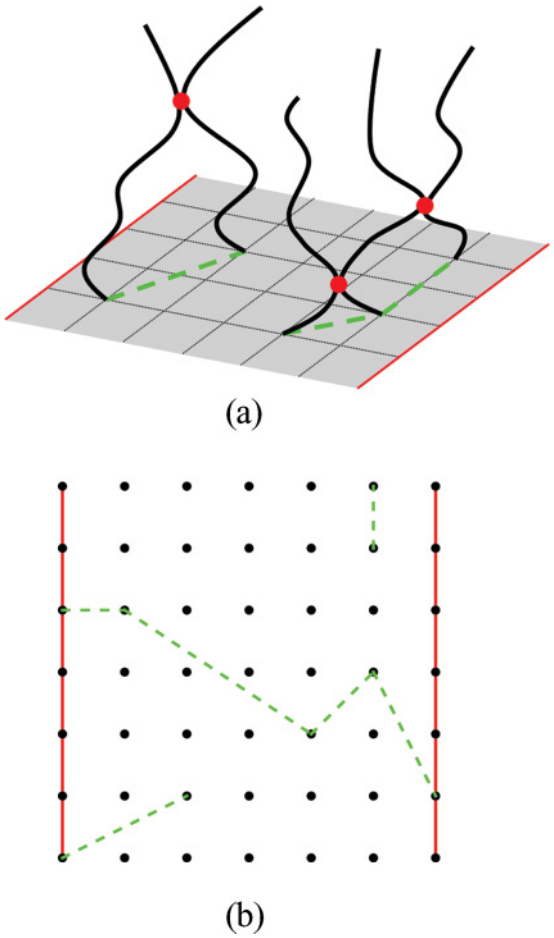

FIG. 1. (Color online) Visualization of the percolation problem for cross-linked polymer brushes. The dashed green lines are examples of how cross-links can connect two grafting points (a). A brush is called percolating if a continuous path of bonds connects two opposite boundaries of the sample (solid red lines) (b).

Each grafted chain is uniquely characterized by its grafting point. Thus, cross-linking can be mapped onto a percolation problem in the 2D lattice of grafting points as shown in Fig. 1(a). Because of this unique relation between the 2D percolation problem and the gelation of polymer brushes, we will use the terms "percolation" and "gelation" synonymously in the following. The percolation analysis of the original BFM simulation of the cross-linked polymer brushes has then been carried out using a cluster coloring algorithm [33] on the 2D grafting lattice after every addition of the next bond from the bond list. This was done until percolation was reached. A sample is called percolating in the x or y direction, if there is a continuous path of bonds that travels across the full sample in the particular direction without crossing the periodic boundaries; see Fig. 1(b).

The mapping on the 2D grafting lattice enables us later to consider much larger systems by reducing all polymer degrees of freedom to a distribution of bond vectors. Only this distribution is taken from the BFM simulations in order to

investigate the gelation properties of the cross-linked brush. We return to the analysis of the percolation problem in Secs. IV and V.

III. NETWORK PROPERTIES AND BOND DISTRIBUTIONS OF CROSS-LINKED POLYMER BRUSHES

A. Primary cross-links, secondary cross-links, and self-links

In order to analyze network features of cross-linked polymer brushes the cross-links are divided into three categories: *Self-links* connect monomers of the same chain, *primary cross-links* link two previously unconnected chains, while *secondary cross-links* are a repeat of an existing bond between a pair of different grafting points.

Typical results for the original bond distribution of the BFM simulations at the particular percolation threshold are shown in Fig. 2 for five samples of chain length $N = 64$ at various grafting densities. The number of added bonds per chain, q, is given by the total number of bonds (one bond connects two monomers) divided by the total number of chains in the system. The theoretical expressions for the lines in the figure are derived in the following sections. The figure shows that the percolation threshold in terms of the number of all bonds added is very high for low grafting densities. For instance, for σ a little above $\sigma^* \approx 0.013$, the added bonds are in their majority self-links, so that the percolation value in terms of primary cross-links is only a small fraction of the total number of network bonds. For higher grafting densities, the number of added bonds at the onset of percolation decreases, mainly because the fraction of self-links decays.

B. Bond distributions and scaling

For the percolation problem, only primary cross-links are important. These primary cross-links can be characterized by the vectors $\vec{v}$ connecting two grafting points. Primary cross-links are characterized by the corresponding pair of grafting points. The bond between is directionless, and due

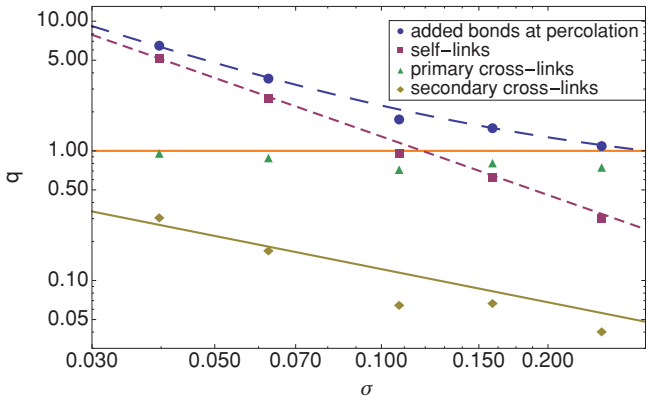

FIG. 2. (Color online) Frequency of occurrence of different types of added bonds at the onset of percolation for $N = 64$. The fraction of primary cross-links is considerably smaller than one bond per chain (indicated by the horizontal solid orange line at $q = 1$), the value expected from classical 2D bond percolation on a square lattice. The theoretical lines are derived and discussed in Sec. III B.

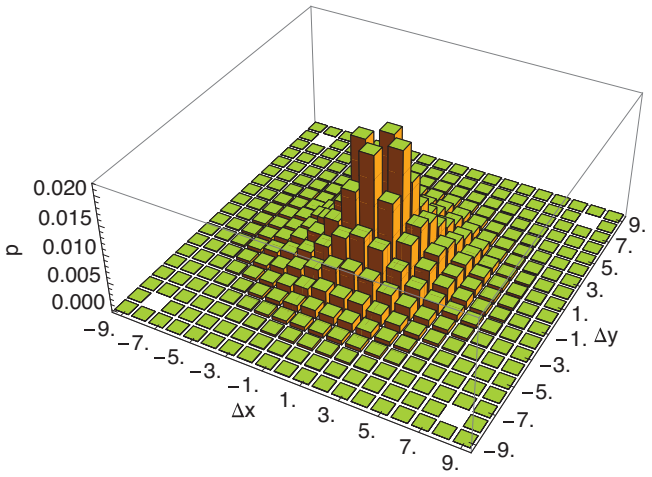

FIG. 3. (Color online) Symmetrized bond distribution for $N = 64$ and $\sigma = 0.25$. The height of the column indicates the frequency with which primary cross-links connecting grafting points with the distance $(\Delta x, \Delta y)$ occur.

to the symmetry of the lattice we can define a *bond class* B of equivalent connections similarly to defining a class of vectors: Two bonds are of the same bond class $B = (\Delta x, \Delta y)$, if the vectors between the particular pair of grafting points differ only by sign permutations of the vector components.

In the following, a *bond distribution* is a collection of all the bond classes present together with their relative frequencies. In Fig. 3 the frequency p of primary cross-links between grafting points in a given direction and distance is shown exemplarily for $N = 64$ and $\sigma = 0.25$.

The cross-linking process leads to a broad bond distribution which decays monotonically with increasing bond length. Numerical tests have shown that the resulting bond distribution can be considered invariant with respect to the number of bonds added to the system. Thus, the bond distribution at the end of the cross-linking can be used, allowing a higher precision in the relative frequencies of the bond classes. This also indicates that correlation effects during the cross-linking process are rather weak. As very long bonds occur only seldom, a reasonable cutoff for each bond distribution is applied individually. In the following, we use the distance between two grafting points as the unit length scale (lattice of grafting points).

In order to analyze the dependence of chain length and grafting density, we consider the distribution of bond lengths $b = |\vec{v}|$. In Fig. 4 we display the bond length distribution $p(b = |\vec{v}|)/p(1)$ at constant grafting density $\sigma = 0.25$ for different chain lengths N. The distribution shows an exponential decay for all chain lengths. The decay decreases with increasing chain length, reflecting the longer range of the bonds. Bond length distributions are shown for fixed chain length $N = 64$ and different grafting densities in Fig. 5. Here, the decay of the distribution is decreasing with increasing grafting density.

The above observations suggest that the bond length distribution is characterized by the average extension of the grafted chain within the lattice of grafting points. For $\sigma \gg \sigma^*$ the chains are represented by a 2D random walk of blobs [21,34]. The size of the blobs is given by the grafting density

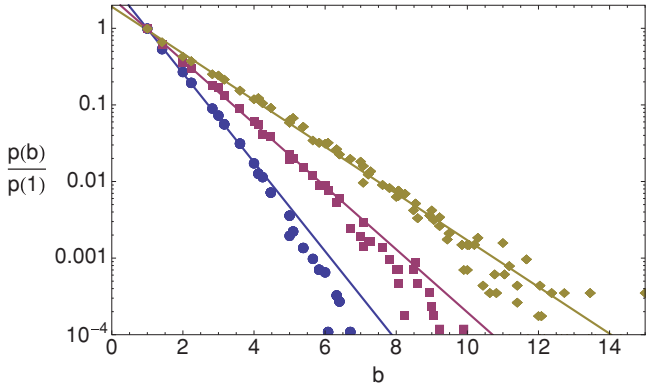

FIG. 4. (Color online) Bond length distribution for $N = 16$ (circles), 32 (squares), and 64 (diamonds) with $\sigma = 0.25$. All distributions show an exponential decay.

as $\xi = \sigma^{-1/2}$ and the number of monomers within a blob is $g \sim \xi^{1/\nu} \sim \sigma^{-1/2\nu}$. Thus, the average lateral extension of a grafted chain in the lattice of grafting points (lattice constant ξ) is given by

$$b_0(N,\sigma) \propto (N/g)^{1/2} \propto \sigma^{5/12} N^{1/2}, \tag{1}$$

where we have used $\nu \approx 3/5$ [35,36]. In Fig. 6 we display the rescaled bond length distributions using b/b_0 as the scaling variable. Here, we used Eq. (1) with the prefactor according to $b_0(64,0.25) = 1$. The data in Fig. 6 are additionally rescaled along the y axis according to $p(1) = 1$ which corresponds to normalization of the rescaled probability density (given an exponential decay). The rescaled data points lie roughly on a master curve. The slope in the semilogarithmic plot is ≈ -0.7 ($N = 64$, $\sigma = 0.25$) for the given choice of the prefactor for b_0. Being of order 1, it shows that this length scale is on the order of the lateral extension b_0 as given in Eq. (1) and thus on the order of the lateral fluctuations of the chains. Deviations for low grafting densities are expected since our scaling argument is valid for $\sigma \gg \sigma^*$ only.

As a result of this analysis we find that the bond distribution depends on universal parameters of the polymer brush. The lateral fluctuations of the conformations of a grafted chain

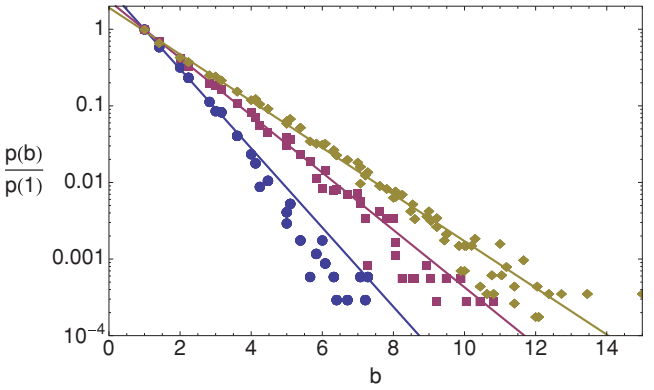

FIG. 5. (Color online) Bond length distribution for $\sigma = 0.04$ (circles), 0.11 (squares), and 0.25 (diamonds) with $N = 64$. All distributions show an exponential decay.

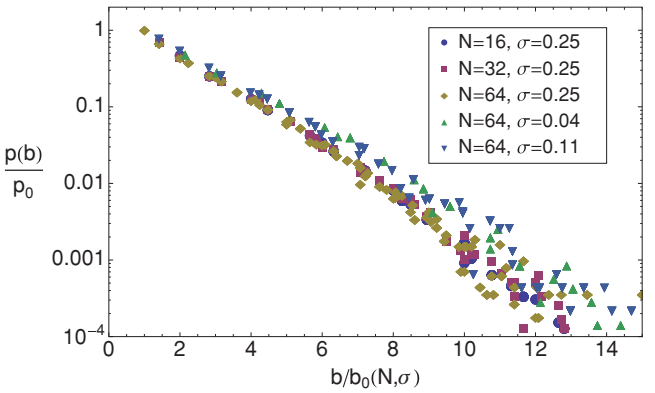

FIG. 6. (Color online) Rescaled bond length distribution of the data in Fig. 4 and 5. The y axis has been rescaled such that all data sets start at (1,1). Almost all data lie on one master curve; the little overlap between chains accounts for the deviations at small grafting densities.

characterize the range of the distribution of bonds. In particular the combination $N\sigma^{1/2\nu}$ controls the cross-linking behavior.

The above scaling arguments can also be applied to derive estimates for self-links and secondary cross-links as shown in Fig. 2. As assumed in Eq. (1), the N/g blobs of the chains inside the brush perform a random walk of N/g steps in the xy direction. Thus, this random walk reaches on the order of N/g different grafting points and the probability to return to the same lattice point is of the order of g/N, which is $\sim g \sim \sigma^{-1/2\nu}$ for the constant N. This prediction is plotted by a solid line in Fig. 2. The amount of self-links at the gel point can be estimated from a comparison of intrachain monomer contacts with interchain contacts. Using similar scaling arguments as above we find that the self-link contribution is roughly proportional to the inverse of the blob volume $\sim \sigma^{-3/2}$ as shown in Fig. 2.

IV. STAR PERCOLATION

The data in Fig. 2 show that the percolation threshold observed in the simulations in terms of the primary cross-links ($q_c \approx 0.75$) drops clearly below $q_c = 1$, the percolation threshold expected from bond percolation in 2D. In order to provide an intuitive explanation for this result we reconsider in this section first the standard bond percolation problem with a bimodal distribution of bond vectors before we proceed to the bond distributions as obtained by BFM simulations in the following section. Due to the starlike pattern of possible bond vectors originating from each site, we call both simulations *star percolation* in the following.

A. Simulation and analysis

Consider any 2D or nD translationally invariant lattice of a given size L that contains no bonds between lattice sites. Assume that the bond distribution $\{(B_i, p_i)\}$ is given, where B_i is a bond class and p_i is the corresponding frequency. Now, the following algorithm is implemented: A bond class B_i is randomly selected according to its statistical weight p_i and a bond vector is created by randomly assigning positive or negative signs to the vector elements $(\Delta x, \Delta y)$. This bond is

added to the lattice at a random position and percolation in the x and y directions is monitored. The above steps (bond creation and insertion) are repeated until percolation is reached and the number of added bonds per lattice site, q, at percolation is recorded.

Repetition of this procedure a number of times leads to a distribution of these lattice-size-dependent values $q(L)$. In the limit of infinite system size, the distribution approaches a step function and the value at which the step occurs is called the percolation threshold q_c.

In the following, P is the cumulative probability for percolation in a lattice with q bonds per point added. The median of the distribution of percolation values characterizes that fraction below which 50% of the cases are already percolating. This value is taken as a lattice-size-dependent percolation value $q_M(L)$. Combining the percolation data in the x and y directions, a finite size scaling [37] is applied, the result of which is the percolation threshold q_c. For finite size scaling, lattices with size $L = 13$ to 97 with $\Delta L = 12$ are used each containing 200 statistically independent samples. For comparison, all system sizes L and bond lengths b are given in lattice units and the percolation threshold q_c is given in units of bonds per lattice point.

B. Star percolation of bimodal bond distributions

While in the original bond percolation problem on a square lattice the bonds all have length $b = 1$ and a maximum of four connections per lattice point is allowed, the more general percolation problem addressed here allows for distribution of bond lengths, direction, and number of bonds per site. We tested these three factors concerning their impact on the percolation threshold using particular bond distributions or limits for the number of bonds per site. Introduction of a length distribution turned out to be the dominating factor, and we discuss the results below using two model distributions of bond lengths.

Two bond distributions are presented in this section, one using bond lengths $b_1 = 1$ and $b_2 = 2$ and the other one using bond lengths $b_1 = 1$ and $b_2 = 3$. The bonds are parallel to the lattice boundaries, making the system comparable to the classic bond percolation problem with bond length $b = 1$. The fraction r of the long bonds with length b_2 is varied so that r changes from 0% to 100% in steps of 10%. The dependence of q_c on the bond length frequency ratio r is shown in Fig. 7 for $b_2 = 2$ and 3.

It can be clearly seen that the percolation threshold drops below $q_c = 1$ as soon as only a small fraction of bonds of other length(s) is involved in the percolation process. The percolation threshold initially decays with increasing fraction of longer bonds in the system. It is remarkable that this dependence is quite asymmetric with respect to $r = 0.5$.

This result can be explained as follows: If only longer bonds are put into the system several sublattices are filled independently. A sublattice in this sense is the set of lattice points that can be reached from one random lattice point while using the longer bond length only. These sublattices can only be connected by bonds of length 1, making it possible to jump from one sublattice to another sublattice on the way from one lattice end to the other. As the longer bonds traverse larger distances, even a small fraction of short bonds is enough to enable the connections between the sublattices and therefore lowers the percolation threshold. As a limiting case, the percolation threshold $q_c = 1$ (classical bond percolation on a 2D square lattice), is obtained if the bond distribution is monodisperse with short bonds only. The slight deviation for monodisperse bond distributions with long bonds only might be explained with not completely filled sublattices.

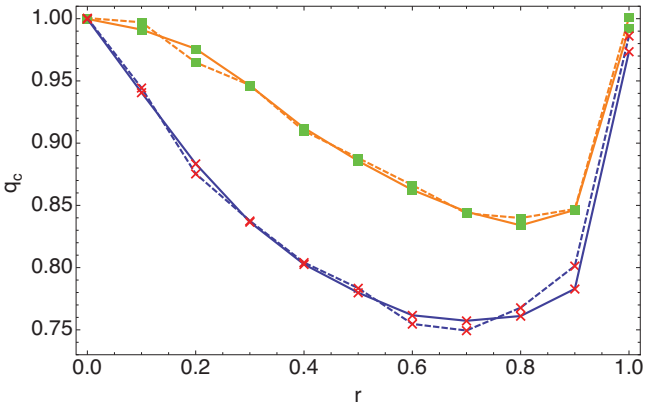

FIG. 7. (Color online) Percolation threshold vs fraction of longer bonds of length $b_2 = 2$ (squares) and 3 (crosses). The percolation threshold shows an asymmetric dependence on the fraction of longer bonds. The dashed curves represent data obtained from finite size scaling on different data sets.

To conclude, we have shown that mixing of bond vectors of different lengths yields a lower percolation threshold as compared to simple bond percolation.

V. STAR PERCOLATION OF POLYMER BRUSHES

The concept of star percolation is used below as a coarse-grained model of cross-linking a polymer brush. This allows us to consider larger systems with given numerical resources without resorting to a direct polymer simulation. The key input from the polymer model is the distribution of bonds in the lattice of grafting sites, which can be obtained from the simulation of rather small systems.

A. Percolation thresholds

Based on the simulations with model bond distributions discussed in the last section, the percolation threshold is expected to drop below $q_c = 1$ for bond distributions obtained from the simulations of the cross-linked polymer brushes. In this section, we now repeat the analysis of the previous section for the star percolation simulations that use the full bond distributions as obtained from the BFM simulations of polymer brushes. The percolation threshold for the cross-linked brush bond distribution is obtained by finite size scaling of the results for lattices ranging from size $L = 13$ to 97 with $\Delta L = 12$ and an ensemble size of 200 each. In Fig. 8 the percolation probability and the percolation threshold are plotted exemplarily for chain length $N = 64$ and grafting density $\sigma = 0.25$. The percolation thresholds for systems with different chain lengths and grafting densities are given in Table I.

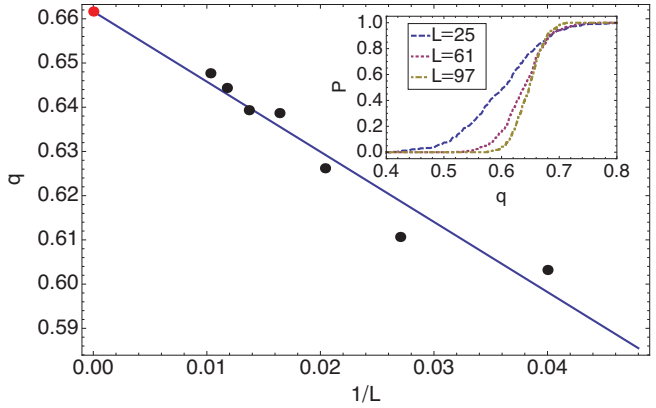

FIG. 8. (Color online) Percolation threshold q_c for chain length $N = 64$ and grafting density $\sigma = 0.25$. Finite size scaling yields $q_c = 0.662$, which is considerably lower than $q_c = 1$ (classical 2D bond percolation). The percolation probability for different lattice sizes is shown as an inset.

As observed in Sec. III B, the bond distribution is controlled by the number of blobs per chain in the polymer brush. Thus, all properties derived from the bond distribution should display the same scaling. In Fig. 9, the percolation threshold from Table I is plotted as a function of the number of blobs per chain. As expected, the data for various grafting densities and chain lengths collapse onto a common master plot. After the data are shifted by -0.5 to reflect the lowest possible percolation threshold $q_c = 0.5$, which is given by mean-field gelation, it can be fitted by a power law with a slope of ≈ -0.42.

Figure 9 indicates a decrease of the percolation threshold with increasing overlap of the grafted chains. As a consequence of the scaling of the bond length distribution, the percolation threshold for a fixed chain length thus decreases with increasing grafting density and also increases with increasing chain length following the scaling behavior according to $N\sigma^{1/2\nu}$.

While star percolation as a coarse-grained model reflects the main features of the cross-linked polymer brush, correlation effects that may occur during the cross-linking process are not included. This is because bonds are drawn randomly from the real distribution of bond lengths. Correlations can occur for several reasons. As an example, chains that connect two grafting points with a large distance on the lattice are bent toward each other to bridge this gap. Bonds that are oriented in the direction of the other chain are possibly preferred to those in the opposite direction. This effect is enhanced at lower grafting densities (on the verge of overlapping). Such effects might be included in the star percolation problem by adding bonds in a correlated fashion.

TABLE I. Percolation thresholds from star percolation for bond distributions obtained from simulations with different chain lengths and grafting densities.

N	σ^*	$\sigma = 0.0625$	$\sigma = 0.11$	$\sigma = 0.16$	$\sigma = 0.25$
16	0.028	0.970	0.905	0.866	0.828
32	0.018	0.864	0.794	0.766	0.726
64	0.013	0.751	0.709	0.683	0.662

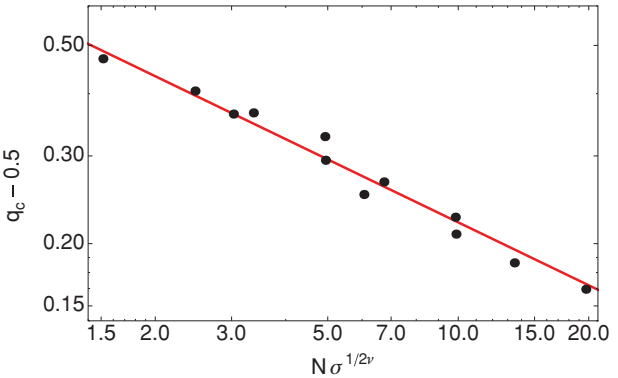

FIG. 9. (Color online) Percolation threshold as a function of $N\sigma^{1/2\nu}$. The data are shifted by -0.5 to reflect the lowest possible percolation threshold $q_c = 0.5$, which is given by mean-field gelation. The slope of the fit is ≈ -0.42.

B. Cluster size distributions

The cluster size distributions as obtained from star percolation using the bond distribution of a cross-linked polymer brush are displayed in Fig. 10 for the case $N = 16$ and $\sigma = 0.25$. The data display a crossover from mean-field to critical behavior with increasing cluster size of about $s_{co} = 18$.

The slope of the initial decay ($s < 18$) is $\tau = 2.48$, which is in good agreement with the slope expected from the mean-field gelation model ($\tau = 2.5$) [38]. An ideally branching cluster of s lattice sites on the 2D lattice resembles the conformations of a lattice animal with lateral spatial extension $R \sim |b|s^{1/4}$. In general, ideal branching becomes impossible, if the growing clusters are dense within their own volume $R^D \approx s$, which is the case for

$$s_{co} \approx |b|^{4D/(4-D)} \sim (N/g)^{2D/(4-D)} \sim (N\sigma^{1/2\nu})^{2D/(4-D)}, \quad (2)$$

with $D = 2$ for cross-linked brushes and $D = 3$ for bulk networks. For the example given in Fig. 10, the bond distribution decays to $1/e$ for $|b| \approx 2$; see Fig. 4. Thus, we obtain a value of 16 in good agreement with the observed crossover value. Bigger clusters ($s > s_{co}$) have to follow restrictions imposed by external space. In this range, the

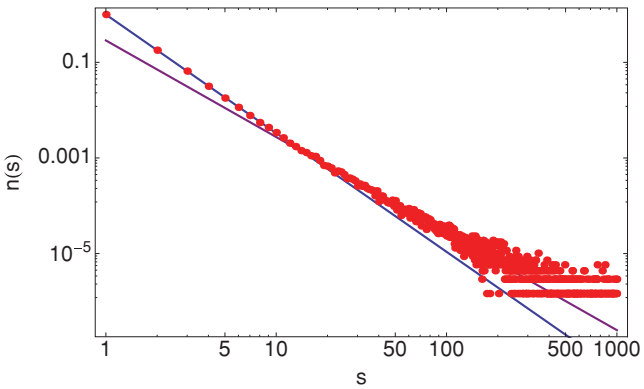

FIG. 10. (Color online) Cluster size distribution for $N = 16$ and $\sigma = 0.25$. The transition from mean-field behavior (slope -2.48 in good agreement with the theoretical value -2.5) to critical behavior (slope -2.02 in good agreement with the theoretical value -2.05) is clearly visible.

exponent changes to $\tau = 2.02$, which is in good agreement with the value expected for 2D percolation ($\tau \approx 2.05$) [39]. We note that for bulk networks, the crossover point is shifted to a rather high value of $s \approx (N/g)^6$, which is difficult to observe for typical values of $N/g \gg 1$. Thus, polymer networks are dominated by mean-field behavior [36].

VI. SUMMARY AND CONCLUSION

We have studied the cross-linking of polymer brushes using Monte Carlo simulations. In contrast to ordinary polymer networks, polymer chains in brushes are ordered on a 2D lattice with respect to one of their end points in our simulations. This allows us to map the cross-linking process into a corresponding 2D percolation problem. The difference between simple bond percolation and the problem at hand is a broad distribution of bond vectors which allow direct bonds between grafting points (sites) at longer distance. We call this variant of percolation "star percolation." The key property for the mapping is the distribution of bonds obtained from the direct simulation. When the bond distribution in the cross-linked polymer brush has been obtained numerically, the gelation process can be studied using the percolation model.

The distribution of bond lengths (distances between grafting points of cross-linked chains) displays an exponential decay which is well characterized by the lateral extension of the grafted chains. More precisely the *overlap* of a given chain with other chains (number of grafting points within the area of a given chain) is characterized by the scaling variable $N\sigma^{1/2\nu}$, and this variable controls the bond distribution for grafting densities well above the overlap threshold. This confirmed scaling behavior can be used to generate the bond distribution without the need for simulations for any combination of N and σ.

Using finite size scaling we have shown that star percolation displays a lower percolation threshold $q_c < 1$ as compared to bond percolation $q_c = 1$. This result agrees with the direct observation of a lower percolation threshold in cross-linked polymer brushes. Moreover, the scaling behavior of the bond distribution is directly transferred to the gelation properties of the polymer brush. As a consequence, the gelation threshold depends on the scaling variable $N\sigma^{1/2\nu}$ only.

The data for the cluster size distribution show a pronounced crossover from the mean-field gelation behavior for small cluster sizes to critical percolation behavior for larger cluster sizes at $s \approx (N/g)^2$. To conclude, we have introduced star percolation as a paradigm to understand the basic features of gelation process in cross-linked polymer brushes.

[1] D. H. Napper, *Polymeric Stabilisation Of Colloidal Dispersions* (Academic Press, London, UK, 1983).
[2] W. B. Russel, D. A. Saville, and W. R. Schowalter, *Colloidal Dispersions* (Cambridge University Press, Cambridge, UK, 1989).
[3] V. P. Torchilin, AAPS J. **9**, E128 (2007).
[4] J. Klein, E. Kumacheva, D. Mahalu, D. Perahia, and L. J. Fetters, Nature (London) **370**, 634 (1994).
[5] J. Klein, D. Perahia, and S. Warburg, Nature (London) **352**, 143 (1991).
[6] T. Moru, Y. Takatori, K. Ishihara, T. Konno, Y. Takigawa, T. Matsushita, U. Chung, K. Nakamura, and H. Kawaguchi, Nat. Mater. **3**, 829 (2003).
[7] B. Zdyrko, V. Klep, X. Li, Q. Kang, S. Minko, X. Wen, and I. Luzinov, Mater. Sci. Eng. C **29**, 680 (2009).
[8] P. Uhlmann, H. Merlitz, J. U. Sommer, and M. Stamm, Macromol. Rapid Commun. **30**, 732 (2009).
[9] P. Uhlmann, N. Houbenov, L. Ionov, M. Motornov, S. Minko, and M. Stamm, Wissenschaft. Z. Tech. Univ. Dresden **1**, 47 (2007).
[10] S. Alexander, J. Phys. (France) **38**, 983 (1977).
[11] P. G. de Gennes, J. Phys. (France) **37**, 1445 (1976).
[12] A. Halperin, M. Tirrell, and T. P. Lodge, Adv. Polym. Sci. **100**, 311992.
[13] A. N. Semenov, Sov. Phys. JETP **61**, 733 (1985).
[14] S. T. Milner, T. A. Witten, and M. E. Cates, Europhys. Lett. **5**, 413 (1988).
[15] P. Y. Lai and K. Binder, J. Chem. Phys. **95**, 9288 (1991).
[16] K. Binder, P. Y. Lai, and J. Wittmer, Faraday Discuss. **98**, 97 (1994).
[17] P. Y. Lai and K. Binder, J. Chem. Phys. **97**, 586 (1992).
[18] M. Murat and G. S. Grest, Macromolecules **22**, 4054 (1989).
[19] G. S. Grest and M. Murat, Macromolecules **26**, 3108 (1993).
[20] G. S. Grest, Macromolecules **27**, 418 (1994).
[21] G. L. He, H. Merlitz, J. U. Sommer, and C. X. Wu, Macromolecules **40**, 6721 (2007).
[22] R. C. Advincula, W. J. Brittain, K. C. Caster, and J. Rühe, *Polymer Brushes. Synthesis, Characterization, Applications* (Wiley-VCH Verlag, Weinheim, Germany, 2004).
[23] Y. Tsujii, K. Ohno, S. Yamamoto, A. Goto, and T. Fukuda, in *Surface Initiated Polymerization I*, Advances In Polymer Science (Springer-Verlag, Berlin, 2006), Vol. 197, pp. 1–45.
[24] L. Guojun, in *Concise Polymeric Materials Encyclopedia* (Bausch & Lomb, Rochester, NY, 1999), pp. 314–316.
[25] G. J. Liu, X. Q. Xu, K. Skupinska, N. X. Hu, and H. Yao, J. Appl. Polym. Sci. **53**, 1699 (1994).
[26] J. U. Sommer, T. A. Vilgis, and G. Heinrich, J. Chem. Phys. **100**, 9181 (1994).
[27] J. U. Sommer and S. Lay, Macromolecules **35**, 9832 (2002).
[28] M. Lang and J. U. Sommer, Phys. Rev. Lett. **104**, 177801 (2010).
[29] M. Lang, D. Göritz, and S. Kreitmeier, Macromolecules **38**, 2515 (2005).
[30] I. Carmesin and K. Kremer, Macromolecules **21**, 2819 (1988).
[31] H. P. Deutsch and K. Binder, J. Chem. Phys. **94**, 2294 (1991).
[32] J. U. Sommer, M. Schulz, and H. L. Trautenberg, J. Chem. Phys. **98**, 7515 (1993).
[33] J. Hoshen and R. Kopelman, Phys. Rev. B **14**, 3438 (1976).
[34] A. Halperin, in *Soft Order in Physical Systems* (Plenum Press, New York, 1994), Vol. 323, pp. 33–56.

[35] P. Flory, *Principles of Polymer Chemistry* (Cornell University Press, Ithaca, NY, 1981).
[36] P. G. de Gennes, *Scaling Concepts in Polymer Physics* (Cornell University Press, Ithaca, NY, 1991).
[37] K. Binder, Z. Phys. B **43**, 119 (1981).
[38] J. W. Essam and K. M. Gwilym, J. Phys. C **4**, L228 (1971).
[39] D. Stauffer, Phys. Rep. **54**, 1 (1979).